Biochemical and Biophysical Research Communications 391 (2010) 198–202

Contents lists available at ScienceDirect

Biochemical and Biophysical Research Communications

journal homepage: www.elsevier.com/locate/ybbrc

Direct observation of unstained wet biological samples by scanning-electron generation X-ray microscopy

Toshihiko Ogura *

Neuroscience Research Institute, National Institute of Advanced Industrial Science and Technology (AIST), Central 2, Umezono, Tsukuba, Ibaraki 305-8568, Japan

ARTICLE INFO

Article history:
Received 26 October 2009
Available online 10 November 2009

Keywords:
Scanning-electron generation X-ray microscopy
Scanning electron microscopy
Biological sample
Unstained wet specimen
Silicon nitride film
Titanium coating
Monte Carlo simulation

ABSTRACT

Analytical tools of nanometre-scale resolution are indispensable in the fields of biology, physics and chemistry. One suitable tool, the soft X-ray microscope, provides high spatial resolution of visible light for wet specimens. For biological specimens, X-rays of *water-window* wavelength between carbon (284 eV; 4.3 nm) and oxygen (540 eV; 2.3 nm) absorption edges provide high-contrast imaging of biological samples in water. Among types of X-ray microscope, the transmission X-ray microscope using a synchrotron radiation source with diffractive zone plates offers the highest spatial resolution, approaching 15–10 nm. However, even higher resolution is required to measure proteins and protein complexes in biological specimens; therefore, a new type of X-ray microscope with higher resolution that uses a simple light source is desirable. Here we report a novel scanning-electron generation X-ray microscope (SGXM) that demonstrates direct imaging of unstained wet biological specimens. We deposited wet yeasts in the space between two silicon nitride (Si_3N_4) films. A scanning electron beam of accelerating voltage 5 keV and current 1.6 nA irradiates the titanium (Ti)-coated Si_3N_4 film, and the soft X-ray signal from it is detected by an X-ray photodiode (PD) placed below the sample. The SGXM can theoretically achieve better than 5 nm resolution. Our method can be utilized easily for various wet biological samples of bacteria, viruses, and protein complexes.

Introduction

Many types of nanometre-scale analytical tools are indispensable in the various fields of science [1–5]. Soft X-ray microscopy provides many advantages over visible light and electron microscopy for observation of living biological samples [6,7]. The soft X-ray microscope enables measurement of specimens in water using X-rays of *water-window* wavelengths between 2.3 and 4.3 nm [6–9], so called because X-rays of these wavelengths are absorbed more strongly by the biological specimen than by the overlying water layer. Soft X-ray microscopes have been developed using *water-window* X-rays [6,7].

Soft X-ray microscopes are of five types: transmission X-ray microscopes [10–13], scanning transmission X-ray microscopes [14,15], X-ray diffraction microscopes [16–19], point projection microscopes [20] and contact X-ray microscopes [21]. Among these, transmission X-ray microscopes offer the highest spatial resolution; using diffractive zone plates, their resolution approaches 15–10 nm [10]. However, they generally require large and complex synchrotron radiation sources [10–13].

Here, we use a scanning-electron generation X-ray microscope (SGXM) [22] to directly observe unstained wet biological specimens. Yeast samples are deposited in Si_3N_4 films on Si window frames (Fig. 1A and Supplementary Figs. 1 and 2). The film top is coated with a layer of titanium (thickness 180 nm), then irradiated by a scanning electron beam (EB) with an accelerating voltage of 5 or 7 keV. Soft X-rays from the titanium layer and transmission electrons (TEs) are both detected by an X-ray photodiode (PD) [23,24] under the sample holder. The electron trajectory in the Ti-coated film is calculated by Monte Carlo (MC) simulation [25].

Materials and methods

Titanium coating on the Si_3N_4 film. The window side of a Si_3N_4 film (50 nm) supported by a window (0.5 × 0.5 mm) in a Si frame (5 × 5 mm; Silson Ltd, UK) was coated with titanium by means of a vacuum deposition unit (MP-61070, JEOL, Japan). A titanium wire (0.15 × 30 mm; Nilaco Co., Japan), was attached to a tungsten filament in the vacuum deposition unit. The deposited titanium layer was approximately 180 nm thick, as determined by SEM imaging (Supplementary Fig. 1D), which is three times the deposition with a heater control level of 90 and 100 for 1 and 3 min, respectively.

Abbreviations: EB, electron beam; ISEC, indirect secondary electron contrast; MC, Monte Carlo; PD, photodiode; SEM, scanning electron microscopy; SE, secondary electron; SGXM, scanning-electron generation X-ray microscopy; Si_3N_4, silicon nitride; TE, transmitted electron; Ti, titanium; 3D, three-dimensional

* Fax: +81 29 861 5065.
E-mail address: t-ogura@aist.go.jp.

0006-291X/$ - see front matter © 2009 Elsevier Inc. All rights reserved.
doi:10.1016/j.bbrc.2009.11.031

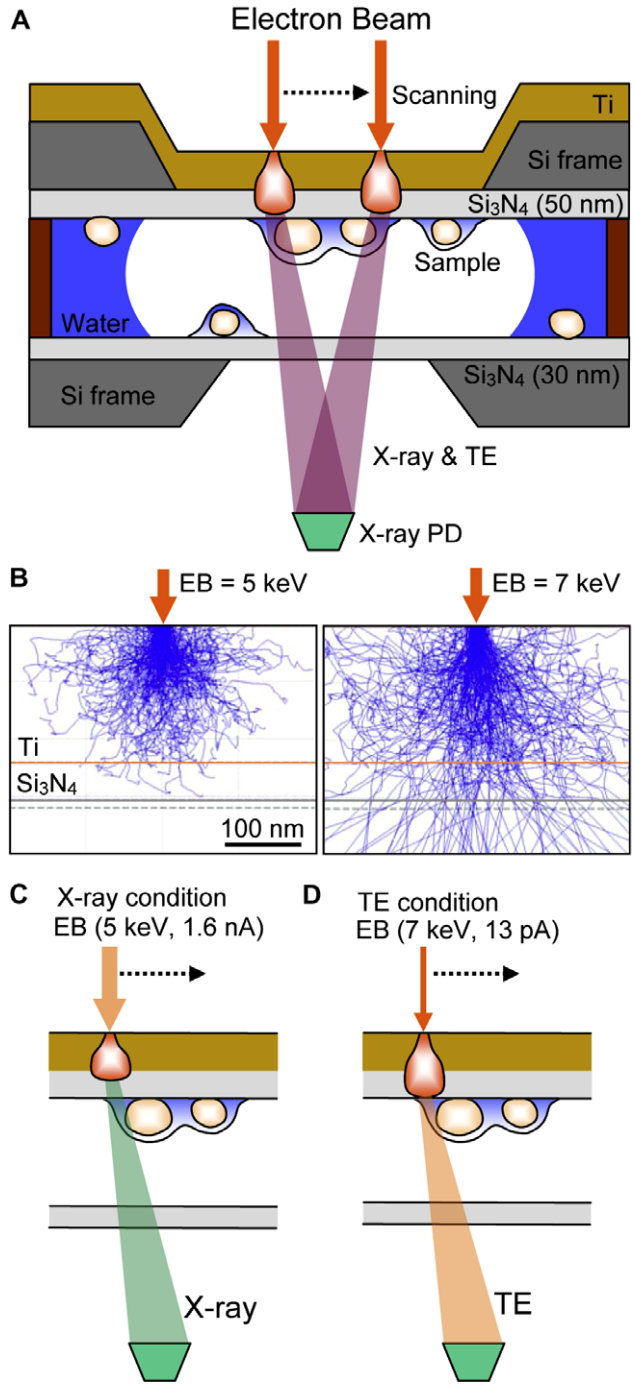

Fig. 1. Experimental setup and data acquisition system. (A) Diagram of the SGXM technique. The scanning EB irradiates the upper side of the Ti-coated Si_3N_4 film. Some scattered electrons reach the lower film surface; in addition, the characteristic X-ray of 453 eV from the Ti layer is emitted. The wet yeasts adsorb onto the Si_3N_4 films in the water drop. An X-ray PD under the sample detects the transmitted X-ray and TE signals and relays them through an amplifier to a data recorder. (B) MC simulation analysis of the Ti-coated Si_3N_4 film, showing the electron trajectory area in the 180-nm Ti layer on the 50-nm Si_3N_4 film. The EB spot diameter is 30 nm. At an EB accelerating voltage of 5 keV, all electrons absorb onto the film (left); at 7 keV, some electrons pass through the film (right). (C) Schematic figure of the X-ray imaging condition (EB accelerating voltage = 5 keV; EB high current = 1.6 nA). (D) Schematic figure of the TE imaging condition (EB accelerating voltage = 7 keV; EB low current = 13 pA).

Sample holder. Ti-coated Si_3N_4 film (50 nm) was attached to a hole (diameter 2.6 mm) in an aluminium holder by carbon tape (Supplementary Fig. 1A–C). Si_3N_4 film (30 nm) supported by a window (0.25 × 0.25 mm) in a Si frame (diameter 3 mm; Structure Probe, Inc., USA) was mounted on the Ti-coated Si_3N_4 by double-sided tape (thickness 10 μm; No. 5601, Nitto Denko Co., Japan). For sample preparation, 2 μl of yeast solution was dropped to the Si frame edge, from where it penetrated the space between the two Si_3N_4 films by surface tension. The frame edges were sealed together by rapid araldite glue (Huntsman Advanced Materials, USA) and the film was dried at room temperature (23 °C) for 2–3 h (Supplementary Fig. 1C).

Sample preparation. A yeast sample of *Sacharomyces cerevisiae* was obtained from DCL Yeast Ltd (UK). Active dried yeast (5 mg) was dissolved in 1 ml of solution containing 0.5% (w/v) trehalose (Hayashibara Inc., Japan), 1.0% glucose and 1.0% NaCl. To ascertain the presence of yeast, a sample solution was observed by optical microscope (400×, Carl Zeiss Axio Observer A1, Germany) before preparation for SEM.

Scanning electron microscopy and X-ray detection system. The wet sample, sealed in Si_3N_4 film, was fixed onto an aluminium stage on the upper side of the Ti-coated Si_3N_4 film (Supplementary Fig. 1B). The stage containing the sample was transferred to the chamber of a thermionic emission SEM (JSM-6390, JEOL, Japan). An X-ray PD [23,24] (AXUV-C20EL, IRD Inc., USA) was fixed under the sample (Fig. 1A and Supplementary Fig. 1B); four PD elements at the detector centre were used for X-ray signal detection (Supplementary Fig. 1E). The signal was amplified by PD preamplifiers, then recorded by data recorder (EZ7510, NF Co., Japan). X-ray and EB scan signals were recorded by data recorder using 16 bits and a 50 kHz sampling range. Data files were then moved to a personal computer. An X-ray image was constructed from the X-ray PD signal according to the EB scan signal, which was calculated by Matlab R2007b (Math Works Inc., USA). SEM images were captured under high vacuum with the following parameters: magnification = 400–5000×; resolution = 1280 × 960 pixels; time = 160 s; working distance = 7 mm; EB accelerating voltages = 5 and 7 keV. The image contrast level of X-ray PD was normalized to black (high intensity) and white (low intensity).

Monte Carlo simulation. Electron trajectories and X-rays generated in the Ti-coated film were calculated by MC simulation using CASINO ver. 2.42 [25]. For the Ti layer, density = 4.5 g/cm^3 and thickness = 180 nm; for the Si_3N_4 film, density = 3.12 g/cm^3 and thickness = 50 nm. Physical models for simulation were the same as in our previous study [26]. Parameters for simulation were as follows: 100,000 electrons; EB accelerating voltages = 5 and 7 keV; EB spot diameter = 30 nm. Simulations were performed on a personal computer (Intel Core2 Duo E6850, 3.0 GHz, Windows XP).

Results and discussion

Our system enables detection of X-ray and TE signals by control of the EB setting (Fig. 1). The X-ray imaging condition is an EB accelerating voltage of 5 keV and high current of 1.6 nA (Fig. 1C). At this condition, irradiated electrons are completely absorbed in the Ti-coated film (Fig. 1B left), the characteristic X-ray of titanium (453 eV, 2.73 nm) [27] is emitted (Supplementary Fig. 3A), and electron damage to the sample is completely prevented. The TE imaging condition is an EB accelerating voltage of 7 keV and low current of 13 pA (Fig. 1D). At this condition, many electrons are transmitted to the film (Fig. 1B right) and TEs are strongly suppressed above 300 nm by the water layer under the Ti-coated Si_3N_4 film (Supplementary Fig. 3B and C). Therefore, the TE imaging condition is used mainly for detection in the water area.

We first observed unstained yeasts in a water drop attached to the space between two Si_3N_4 films (Fig. 2 and Supplementary Fig. 2). The secondary electron (SE) image of the sample, when observed by an original SEM detector under the TE imaging condition

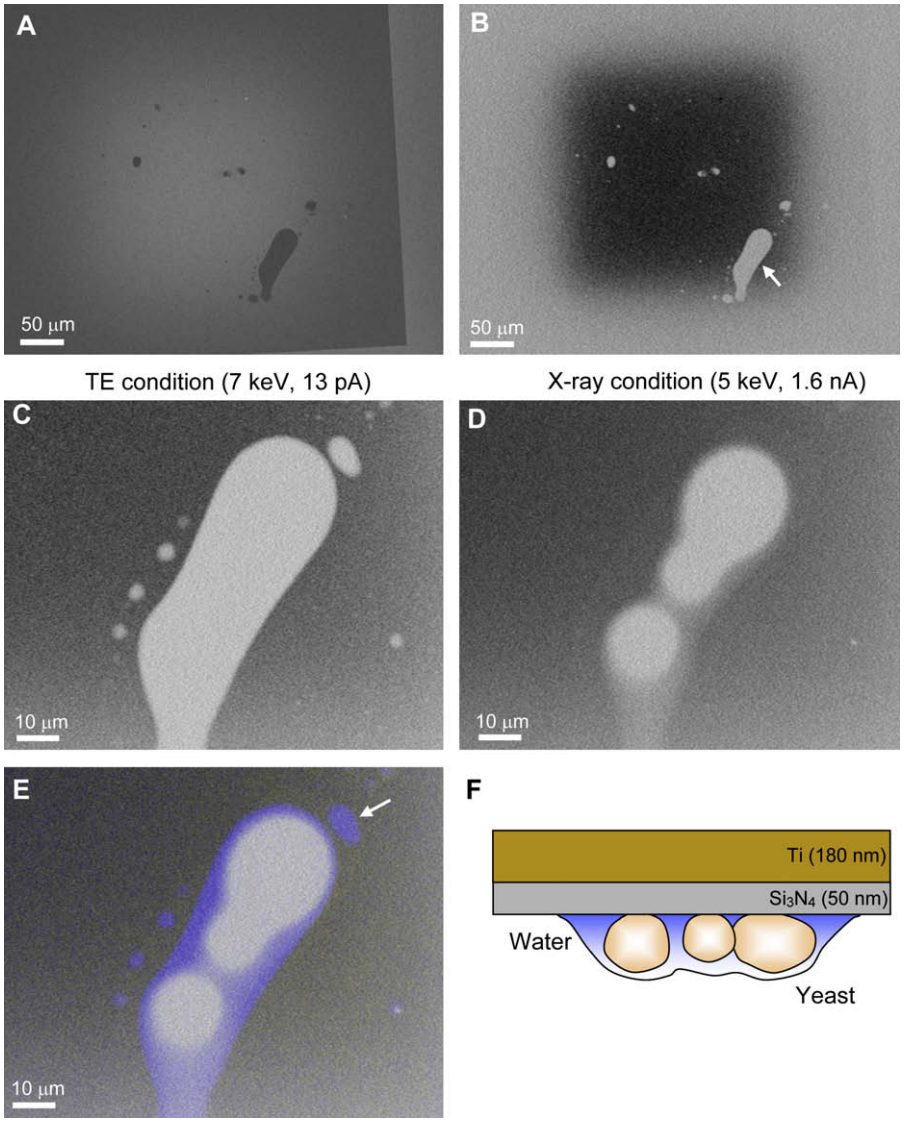

Fig. 2. Images of unstained wet yeast samples taken under X-ray and TE imaging conditions. (A) SE image, detected by an original SEM SE detector, taken under the TE imaging condition (EB accelerating voltage = 7 keV; EB low current = 13 pA). The black areas are droplets. (B) Image of the same sample, detected by an X-ray PD, taken under the TE imaging condition. The white areas are droplets. (C) Large elongated water drop region (arrow in (B)), scanned at 1000× magnification, taken under the TE imaging condition. (D) Image of the same area as for (C), taken under the X-ray imaging condition (EB accelerating voltage = 5 keV; EB high current = 1.6 nA). The image clearly shows yeasts in a water drop. (E) Superimposition of images taken under X-ray and TE imaging conditions (C) and (D). The blue region shows droplets obtained under the TE imaging condition; the white arrow points to a droplet without a yeast sample. (F) Schematic image of the unstained yeast in a water drop based on (E). Scale bars: (A) and (B) 50 μm; (C–E) 10 μm.

(Fig. 2A), shows light areas against the dark contrast of the water drop, much as we describe in our previous report of indirect secondary electron contrast (ISEC) [26,28]. The SE image of the sample, when observed by an X-ray PD under the TE imaging condition (Fig. 2B), shows dark areas against the light contrast of the water drop. A large elongated water drop region (Fig. 2B arrow) scanned at 1000× magnification shows several small droplets scattered about the periphery of the large drop (Fig. 2C). When an image is taken under the X-ray imaging condition (Fig. 2D), yeasts in the drop are clearly evident and the peripheral blobs are disappeared. The image consists of the *water-window* X-ray of 453 eV; the signal is transmissive at the water layer and strongly absorbed by the biological specimen. When the images from Fig. 2C and D are superimposed (Fig. 2E), the yeasts in the water drop become evident, and peripheral blobs (Fig. 2E arrow) consist of solution without biological samples. Fig. 2F shows a schematic image of the observed yeast.

We next observed another water drop at 5000× magnification (Fig. 3). An image taken under the TE condition shows a circular droplet of 10 μm diameter (Fig. 3A). An image taken under the X-ray imaging condition shows an ellipsoid yeast (Fig. 3B). When these images are superimposed (Fig. 3C), the yeasts become evident. To investigate details of the yeast image, we created a pseudo-color 3D map of the image taken under the X-ray imaging condition (Fig. 3D). The yeast is mesa-shaped, because the biological sample strongly absorbs *water-window* X-rays. The centre of the yeast is slightly dented, as is clearly evident from a line plot of the yeast centre (Fig. 3E) and an expanded pseudo-color map (Fig. 3F). These results may suggest that X-ray image intensity reflects sample volume. Therefore, our method would enable reconstruction of a 3D model using a tilting stage.

Finally, we estimated the spatial resolution of the SGXM image by a simple theoretic model and associated equation (Fig. 4 and Eq. (1)). In the actual system, for an EB accelerating voltage of 5 keV

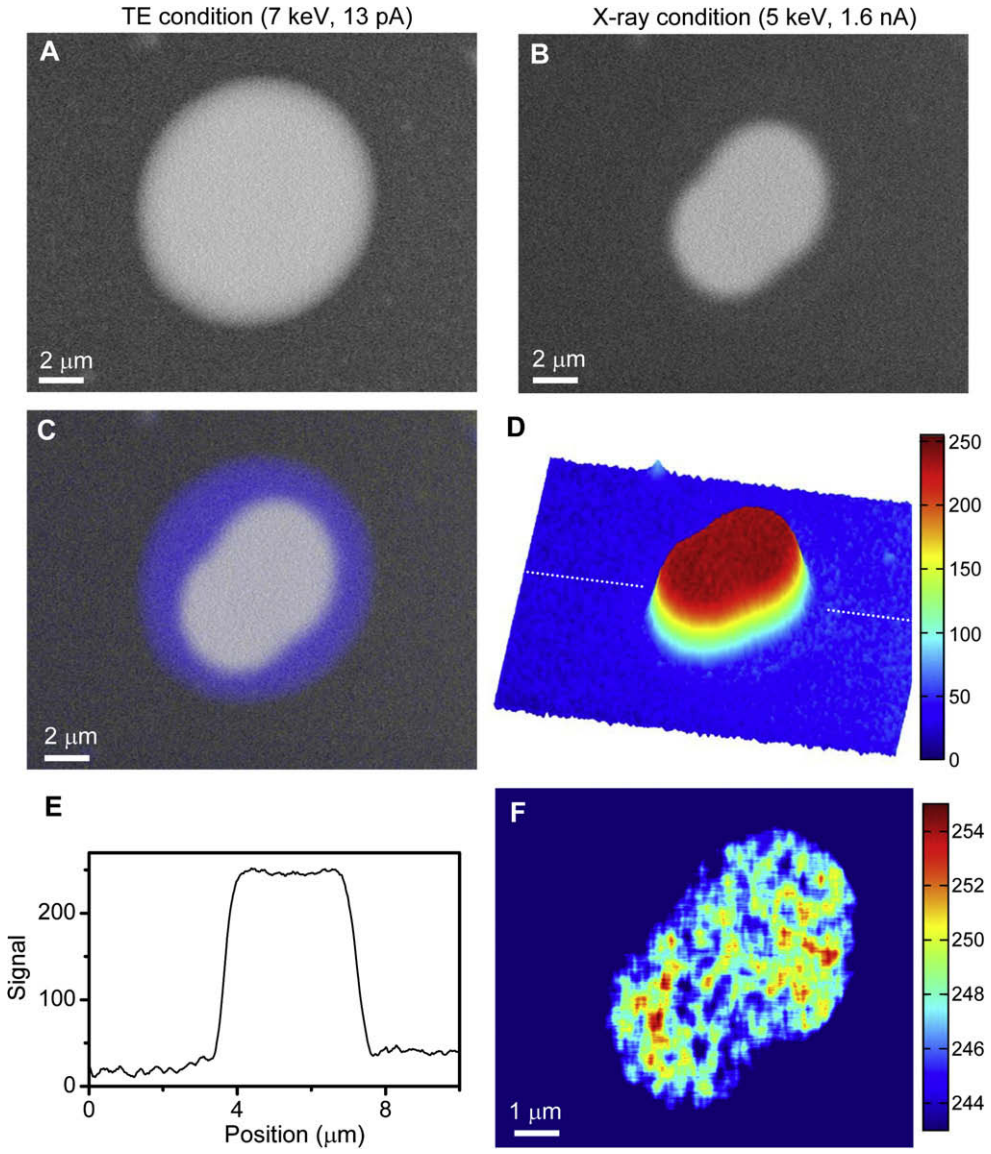

Fig. 3. Analysis of the wet yeast sample by SGXM. (A) Droplet image, detected by X-ray PD, taken under the TE imaging condition at 5000× magnification. (B) Yeast image in the same area, taken under the X-ray imaging condition. (C) Superimposition of images taken under X-ray and TE imaging conditions (A,B). (D) 3D map of a wet yeast taken under the X-ray imaging condition in (B). The body of the yeast is mesa-shaped. (E) Line plot of the centre of the yeast at the white-dash line in (D), filtered beforehand by a 2D Gaussian filter (size = 21 × 21 pixels; σ = 15). (F) Expanded pseudo-color image of a yeast in (B), filtered beforehand by a 2D Gaussian filter (size = 21 × 21 pixels; σ = 15). The centre of the yeast is slightly dented. Scale bars: (A–C) 2 μm; (F) 1 μm.

and spot diameter of approximately 30 nm as determined by thermionic-type SEM, the scattered electron area within the titanium layer is 38 nm as determined by MC simulation (Supplementary Fig. 3A). The soft X-ray source size is approximately the same as the scattered electron density in the titanium layer, because the soft X-ray is generated and emitted mainly from the titanium layer under the X-ray imaging condition. The X-ray detection area expands gradually at positions deeper from the X-ray emission point in the Ti-coated film, until its size finally reaches the sensor width (Fig. 4A). Assuming that spatial resolution R is matched to the X-ray detection area, which is calculated from the detection area and depends on depth L, the relationship can be expressed as:

$$R = (S - D)\frac{(W + L)}{(W + L')} + D, \quad (1)$$

where S is the X-ray detector size, D is the X-ray emission area in the titanium layer, W is the thickness of the Si_3N_4 film and L' is the distance between detector and Ti-coated Si_3N_4 film. R can thus be calculated from L. Fig. 4B shows SGXM spatial resolutions for the actual system and the prediction maximum. In the actual system, at depths less than 100 nm, R approaches 73 nm; at a depth of 1 μm (1000 nm), R is 285 nm (Fig. 4B black line).

R can be improved by a sharper EB and smaller X-ray detector (Fig. 4A right). In particular, the EB spot diameter is highly improved by field emission SEM, and can be readily reduced to smaller than 1.0 nm. For a 50-nm titanium layer irradiated by an EB spot diameter of 1.0 nm, the electron scattering area is approximately 1.4 nm as determined by MC simulation (Supplementary Fig. 4); the X-ray emitting size is fixed to the wavelength of the Ti-characteristic X-ray at 2.73 nm. When a small X-ray detector (0.1 × 0.1 mm) is placed 50 mm below the Ti-coated film, the predicted resolution maximum is higher than 5 nm at below 1 μm depth (Fig. 4B, red line) and better than 10 nm at below 4 μm depth. Therefore, the SGXM can be used for whole cell imaging at better than 10 nm resolution. Theoretical predictions suggest that it can achieve 5 nm resolution, better than previous X-ray microscopes [10].

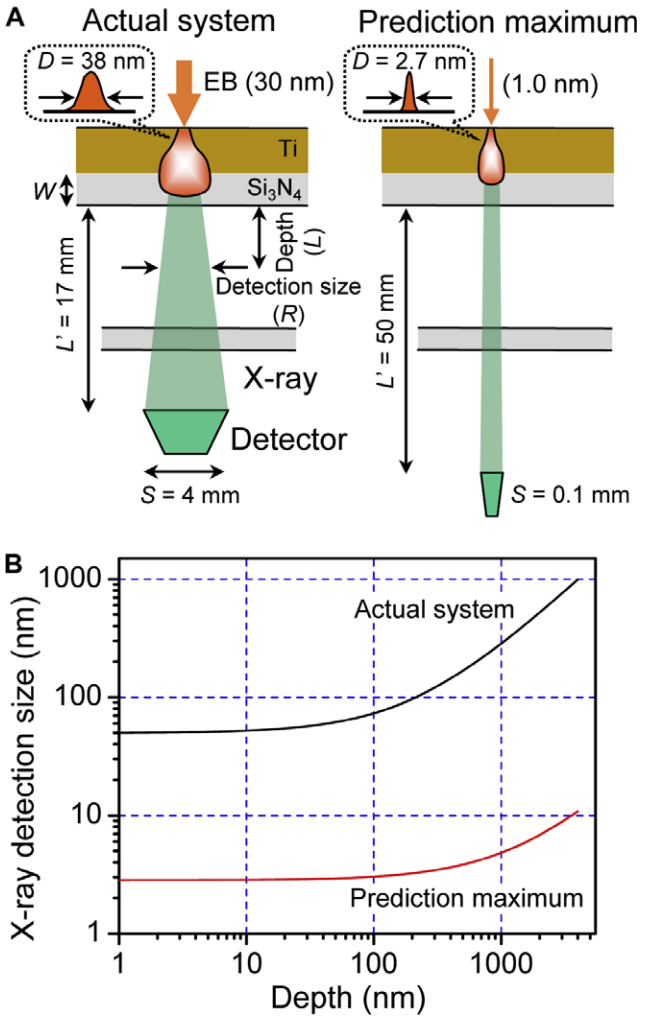

Fig. 4. Theoretical analysis of SGXM spatial resolution. (A) Actual SGXM system (left). The EB spot diameter is 30 nm, as determined by thermionic-type SEM. The electron trajectory area in the Ti layer is approximately 38 nm, as determined by MC simulation. When an X-ray PD (4 × 4 mm) is placed 17 mm below the Ti-coated film, the X-ray detection size increases gradually at deeper positions. For the ultimate SGXM system, the smallest theoretical size of the EB spot diameter (right) is 1.0 nm as determined by field emission SEM; the smallest theoretical electron trajectory size is estimated to be 1.4 nm; the X-ray emitting size is fixed to a wavelength of 2.73 nm; and an X-ray PD (0.1 × 0.1 mm) is placed 50 mm below the Ti-coated film. (B) Estimated SGXM spatial resolutions for the actual and ultimate systems. For the actual system (black line), spatial resolution is better than 73 nm at depths below 100 nm. For the ultimate system (red line), spatial resolution is better than 5 nm at depths below 1 μm.

Conclusion

We measured a wet yeast sample by SGXM. The unstained wet sample under Ti-coated Si_3N_4 film was detected by a soft X-ray signal using a bottom X-ray PD with an EB accelerating voltage of 5 keV and high current of 1.6 nA. The resulting images clearly show yeasts in a water drop. Spatial resolution can theoretically reach better than 5 nm. Our method can be utilized easily for various wet biological samples of bacteria, viruses, and protein complexes.

Acknowledgments

We thank Dr. Y. Fujiyoshi for valuable discussions. This work was supported by KAKENHI Grant-in-Aid for Scientific Research (B) from the Japan Society for the Promotion of Science and by PRESTO of the Japan Science and Technology Agency.

Appendix A. Supplementary data

Supplementary data associated with this article can be found, in the online version, at doi:10.1016/j.bbrc.2009.11.031.

References

[1] A. Sali, R. Glaeser, T. Earnest, W. Baumeister, From words to literature in structural proteomics, Nature 422 (2003) 216–225.
[2] O. Medalia, I. Weber, A.S. Frangakis, D. Nicastro, G. Gerisch, W. Baumeister, Macromolecular architecture in eukaryotic cells visualized by cryoelectron tomography, Science 298 (2002) 1209–1213.
[3] M. Koshino, T. Tanaka, N. Solin, K. Suenaga, H. Isobe, E. Nakamura, Imaging of single organic molecules in motion, Science 316 (2007) 853.
[4] J.C. Meyer, C.O. Girit, M.F. Crommie, A. Zettl, Imaging and dynamics of light atoms and molecules on graphene, Nature 454 (2008) 319–322.
[5] E. de Smit, I. Swart, J.F. Creemer, G.H. Hoveling, M.K. Gilles, T. Tyliszczak, P.J. Kooyman, H.W. Zandbergen, C. Morin, B.M. Weckhuysen, F.M.F. de Groot, Nanoscale chemical imaging of a working catalyst by scanning transmission X-ray microscopy, Nature 456 (2008) 222–225.
[6] J. Kirz, C. Jacobsen, M. Howells, Soft X-ray microscopes and their biological applications, Q. Rev. Biophys. 28 (1995) 33–130.
[7] C. Jacobsen, Soft X-ray microscopy, Trends Cell Biol. 9 (1999) 44–47.
[8] C. Jacobsen, J. Kirz, S. Williams, Resolution in soft X-ray microscopes, Ultramicroscopy 47 (1992) 55–79.
[9] D. Sayre, J. Kirz, R. Feder, D.M. Kim, E. Spiller, Transmission microscopy of unmodified biological materials: comparative radiation dosages with electrons and ultrasoft X-ray photons, Ultramicroscopy 2 (1977) 337–349.
[10] W. Chao, B.D. Harteneck, J.A. Liddle, E.H. Anderson, D.T. Attwood, Soft X-ray microscopy at a spatial resolution better than 15 nm, Nature 435 (2005) 1210–1213.
[11] G. Schneider, Cryo X-ray microscopy with high spatial resolution in amplitude and phase contrast, Ultramicroscopy 75 (1998) 85–104.
[12] C.A. Larabell, M.A. Le Gros, X-ray tomography generates 3-D reconstructions of the yeast, *Saccharomyces cerevisiae*, at 60-nm resolution, Mol. Biol. Cell 15 (2004) 957–962.
[13] A.P. Hitchcock, J.J. Dynes, G. Johansson, J. Wang, G. Botton, Comparison of NEXAFS microscopy and TEM-EELS for studies of soft matter, Micron 39 (2008) 311–319.
[14] S. Williams, C. Jacobsen, J. Kirz, J. Maser, S. Wirick, X. Zhang, H. Ade, M. Rivers, Instrumentation developments in scanning soft X-ray microscopy at the NSLS, Rev. Sci. Instrum. 66 (1995) 1271–1275.
[15] X. Zhang, R. Balhorn, J. Mazrimas, J. Kirz, Mapping and measuring DNA to protein ratios in mammalian sperm head by XANES imaging, J. Struct. Biol. 116 (1996) 335–344.
[16] J. Miao, P. Charalambous, J. Kirz, D. Sayre, Extending the methodology of X-ray crystallography to allow imaging of micrometre-sized non-crystalline specimens, Nature 400 (1999) 342–344.
[17] D. Shapiro, P. Thibault, T. Beetz, V. Elser, M. Howells, C. Jacobsen, J. Kirz, E. Lima, H. Miao, A.M. Neiman, D. Sayre, Biological imaging by soft X-ray diffraction microscopy, Proc. Natl. Acad. Sci. USA 102 (2005) 15343–15346.
[18] C. Song, H. Jiang, A. Mancuso, B. Amirbekian, L. Peng, R. Sun, S.S. Shah, Z. Zhou, T. Ishikawa, J. Miao, Quantitative imaging of single, unstained viruses with coherent X rays, Phys. Rev. Lett. 101 (2008) 158101.
[19] P. Thibault, M. Dierolf, A. Menzel, O. Bunk, C. David, F. Pfeiffer, High-resolution scanning X-ray diffraction microscopy, Science 321 (2008) 379–382.
[20] S.C. Mayo, T.J. Davis, T.E. Gureyev, P.R. Miller, D. Paganin, A. Pogany, A.W. Stevenson, S.W. Wilkins, X-ray phase-contrast microscopy and microtomography, Opt. Express 11 (2003) 2289–2302.
[21] T. Tomie, H. Shimizu, T. Majima, M. Yamada, T. Kanayama, H. Kondo, M. Yano, M. Ono, Three-dimensional readout of flash X-ray images of living sperm in water by atomic-force microscopy, Science 252 (1991) 691–693.
[22] T. Ogura, Measurement of the unstained biological sample by a novel scanning electron generation X-ray microscope based on SEM, Biochem. Biophys. Res. Commun. 385 (2009) 624–629.
[23] E.M. Gullikson, R. Korde, L.R. Canfield, R.E. Vest, Stable silicon photodiodes for absolute intensity measurements in the VUV and soft X-ray regions, J. Electron Spectrosc. Relat. Phenom. 80 (1996) 313–316.
[24] H.O. Funsten, D.M. Suszcynsky, S.M. Ritzau, R. Korde, Response of 100% internal quantum efficiency silicon photodiodes to 200 eV–40 keV electrons, IEEE Trans. Nucl. Sci. 44 (1997) 2561–2565.
[25] D. Drouin, A.R. Couture, D. Joly, X. Tastet, V. Aimez, R. Gauvin, CASINO V2.42—a fast and easy-to-use modeling tool for scanning electron microscopy and microanalysis users, Scanning 29 (2007) 92–101.
[26] T. Ogura, Analyzing indirect secondary electron contrast of unstained bacteriophage T4 based on SEM images and Monte Carlo simulations, Biochem. Biophys. Res. Commun. 380 (2009) 254–259.
[27] B.L. Henke, E.M. Gullikson, J.C. Davis, X-ray interactions: photoabsorption, scattering, transmission, and reflection at E = 50–30,000 eV, Z = 1–92, Atom. Data Nucl. Data Tables 54 (1993) 181–342.
[28] T. Ogura, A high contrast method of unstained biological samples under a thin carbon film by scanning electron microscopy, Biochem. Biophys. Res. Commun. 377 (2008) 79–84.